Aqueous-Solution Growth of GaP and InP Nanowires: A General Route to Phosphide, Oxide, Sulfide, and Tungstate Nanowires

Yujie Xiong,[a, b] Yi Xie,*[a, b] Zhengquan Li,[b] Xiaoxu Li,[b] and Shanmin Gao[b]

Abstract: A general synthetic route has been developed for the growth of metal phosphide, oxide, sulfide, and tungstate nanowires in aqueous solution. In detail, cetyltrimethylammonium cations (CTA^+) can be combined with anionic inorganic species along a co-condensation mechanism to form lamellar inorganic–surfactant intercalated mesostructures, which serve as both microreactors and reactants for the growth of nanowires. For example, GaP, InP, γ-MnO_2, ZnO, SnS_2, ZnS, $CdWO_4$, and $ZnWO_4$ nanowires have been grown by this route. To the best of our knowledge, this is the first time that the synthesis of GaP and InP nanowires in aqueous solution has been achieved. This strategy is expected to extend to grow nanowires of other materials in solution or by vapor transport routes, since the nanowire growth of any inorganic materials can be realized by selecting an appropriate reaction and its corresponding lamellar inorganic–surfactant precursors.

Keywords: cetyltrimethylammonium bromide · gallium · indium · nanostructures · phosphorus · surfactants

Introduction

Controlling the shape of nanostructures at the mesoscopic level is one of the most challenging issues presently faced by synthetic inorganic chemists, since dimensionality plays a critical role in determining the physical properties of materials.[1] One-dimensional (1D) nanostructures such as wires, rods, belts, and tubes, whose lateral dimensions fall anywhere in the range of 1 to 100 nm, have become the focus of intensive research, owing to their unique applications in mesoscopic physics and fabrication of nanoscale devices. In the past decade, significant progress of nanowire growth has been made, with respect to improved uniformity, fine monodispersion, and high yield of products. In detail, nanowires have been grown by many methods, such as electrochemistry,[2] templates (mesoporous silica, carbon nanotubes, etc.),[3] emulsion or polymetric systems,[4] arc discharge,[5] laser-assisted catalyic growth,[6] solution,[7] vapor transport,[8] and organometallic and coordination chemistry methods.[9] Generally, nanowires of the most important inorganic materials have unique growth mechanisms as well as synthetic routes (chemical or physical approach).[10] Despite these exciting developments, a general synthetic strategy to grow nanowires is still significant to both nanotechnology and fundamental research.

Among these important inorganic materials, group IIIA phosphide nanocrystalline semiconductors have been of interest, because of their fundamental physical properties with large direct energy gaps, as well as their potential applications in high-speed digital circuits, microwave devices, and optoelectronics.[11] Compared to the I-VII and II-VI semiconductors, the IIIA phosphides have a greater degree of covalent bonding, a less ionic lattice, and larger exciton diameters. Recently, there have been considerable efforts to explore new routes to synthesize IIIA phosphide nanowires or nanorods, including laser catalytic growth,[12] vapor deposition,[13] sublimation,[14] and carbon nanotube template[15] methods. The solution route is also an effective way to prepare nanowires; Buhro et al. have pioneered the solution-liquid-solid (SLS) model for InP nanowhiskers with diameters ranging from 20 to 200 nm.[16] Cheon et al.[17] also successfully grew GaP nanorods by means of thermal decomposition of a single molecular precursor tris(di-*tert*-butylphosphino)gallane ($Ga(P^tBu_2)_3$) in a hot mixture of amine stabilizers (liquid phase) at 330 °C. Banin et al.[18] reported the synthesis of InP nanorods from the reaction between tris(trimethylsilyl)phosphine ($(TMS)_3P$) and $InCl_3$ in trioctylphosphine oxide (TOPO) with gold nanoparticles as catalysts at 360 °C. From the green chemistry point of view, water is an

[a] Dr. Y. Xiong, Prof. Y. Xie
Structure Research Laboratory
University of Science and Technology of China
Hefei, Anhui 230026 (China)
Fax: (+86) 551-360-3987
E-mail: yxielab@ustc.edu.cn

[b] Dr. Y. Xiong, Prof. Y. Xie, Dr. Z. Li, X. Li, Dr. S. Gao
Department of Chemistry
University of Science and Technology of China
Hefei, Anhui 230026 (China)
E-mail: yxielab@ustc.edu.cn

DOI: 10.1002/chem.200305569

ideal media for the solution route to IIIA phosphide nanowires, driving us to explore the possibility of growing IIIA phosphide nanowires in aqueous solution under mild conditions.

Herein, GaP and InP nanowires have been synthesized in aqueous solution for the first time. This route has also been extended for the growth of γ-MnO_2, ZnO, SnS_2, ZnS, $CdWO_4$, and $ZnWO_4$ nanowires.

Results and Discussion

Before we discuss our experimental results, we will introduce our general strategy for the synthesis of metal phosphide, oxide, sulfide, and tungstate nanowires in aqueous solution.

General route for metal phosphide, oxide, sulfide, and tungstate nanowires: Our present work was enlightened by the "step-edge decoration"[19] model of growing nanowires, in which nanowires form at step edges of substrate surface when removed from the embedding polymer film. Analogously, nanowires should also be grown on the edge of lamellar inorganic–surfactant intercalated mesostructures, since their interlayer interaction can be diminished from the edges under appropriate conditions and lamellar sheets will be rolled into separate scrolls to serve as microreactors. These lamellar mesostructures can form by means of a co-condensation mechanism of inorganic species with ionic surfactant molecules, in the presence of appropriate ratio of surfactant, water, oil, and co-surfactant.

A recent work[20] of Li group confirms the above idea: they showed that $[CTA]_2^{2+}[WO_4]^{2-}$ (CTA^+ = cetyltrimethylammonium cation) lamellar compounds can serve as single precursors for the growth of tungsten and its oxide nanowires by pyrolysis (above 700 °C) in a tube furnace. However, a single-precursor pyrolysis technique is only appropriate for the nanowire growth of few materials. Herein, a general strategy was put forward for the growth of nanowires: a one-pot aqueous solution reaction is established that can produce the target products, in which one of reactants can be combined with ionic surfactant molecules to form lamellar inorganic–surfactant intercalated compounds in aqueous solution. The lamellar compounds can act as both microreactors and reactants in the designed reaction. Hence, the nanowire growth of any material will be realized, as long as an appropriate reaction and its corresponding lamellar inorganic–surfactant precursors can be found. This strategy can also be extended to the vapor transport technique, if it is more to synthesize the appropriate the target materials by means of vapor-phase reactions, in which the lamellar inorganic–surfactant compounds also act as both microreactors and reactants.

The growth model for nanowires by means of the present solution route can be proposed as follows (Scheme 1).

1) Lamellar inorganic–surfactant intercalated mesostructures form through a co-condensation mechanism of inorganic with ionic surfactant molecules. In this work, the cationic surfactant cetyltrimethylammonium bromide (CTAB) and anionic inorganic species were chosen as units to form lamellar inorganic–surfactant intercalated compounds. The lamellar mesostructures, which form before the subsequent reactions, can be characterized by low-angle X-ray diffraction (LA-XRD) patterns.
2) Along with the reactions with other reactants in solution, the lamellar sheets began to loose at the edges and then rolled into separate scrolls.
3) Since the reactant of inorganic species was fixed in lamellar mesostructures, other reactants would be transported from the solution into the scrolls with heat movement of molecules. The scrolls should serve as microreactors, in which the solution reactions took place and produced the final nanowires of target products.

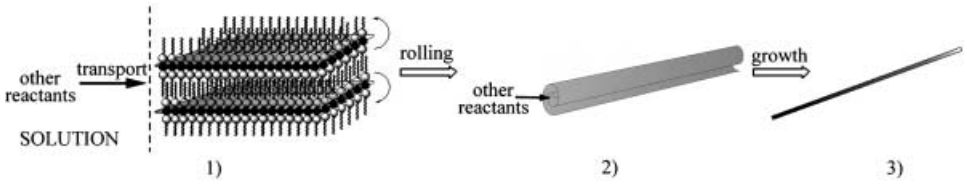

Scheme 1. Schematic formation illustration for the nanowire growth from lamellar inorganic–surfactant mesostructures. The dark dots in lamellar mesostructures represent inorganic species, and the light dots correspond to the CTA^+ ions.

Special case of each as-desired material

Metal phosphide: Our previous research[21] indicates that GaP and InP nanoparticles can be synthesized in aqueous system, taking advantage of the reaction of $M(OH)_4^-$ (M = Ga, In) with PH_3, which was produced from the white phosphorus dismutation in alkali solutions. Based on the above general strategy, $M(OH)_4^-$ should be a good candidate of anionic inorganic species that will most probably participate in constructing lamellar inorganic–surfactant intercalated mesostructures. By selecting the appropriate ratio of CTAB, water, oil, and *n*-hexanol, CTA^+ can be combined with $M(OH)_4^-$ ions to give $[CTA]^+[M(OH)_4]^-$ lamellar mesostructures. Thus a novel aqueous solution route was put forward to grow GaP and InP nanowires. The main reaction process are given in Equations (1)–(3).

$$CTA^+ + M(OH)_4^- \rightarrow [CTA]^+[M(OH)_4]^- \quad (1)$$

$$P_4 + 3\,OH^- + 3\,H_2O \rightarrow PH_3 + 3\,H_2PO_2^- \quad (2)$$

$$[CTA]^+[M(OH)_4]^- + PH_3 \rightarrow MP + 3\,H_2O + OH^- + CTA^+ \quad (3)$$

The $[CTA]^+[M(OH)_4]^-$ lamellar inorganic–surfactant mesostructures have been characterized by low-angle X-ray

diffraction (LA-XRD) patterns. The inset of Figure 1A shows a typical low-angle XRD pattern of the lamellar mesostructures, which were obtained by maintaining the solution of CTAB, $Ga(OH)_4^-$, water, *n*-hexanol, and *n*-heptane in an autoclave at 160 °C for 24 h without adding other reactants. The peaks in the low-angle XRD pattern can be indexed as the (001) and (002) reflections of a lamellar mesophase, indicating that the intermediate of lamellar inorganic–surfactant mesostructures forms in the formation process of GaP or InP nanowires.

The phase and purity of as-obtained nanowires were determined from the X-ray diffraction (XRD) pattern, shown in Figure 1A and B. All the reflection peaks can be indexed to the pure zinc blende (cubic) structure of GaP (JCPDS card 12–191, $a = 5.448$ Å) and InP (32–452, $a = 5.869$ Å), respectively. No characteristic peaks were observed for other impurities, such as Ga_2O_3 and In_2O_3. Compared with that of bulk materials, the intensity of the (111) diffraction peak decreases to 80 % of standard data and its width is slightly narrower than that of the others. This most probably results from the fact that most of nanowires lie on a silicon slice, that the crystal planes perpendicular to nanowire growth axis have a small diffraction probability, and that the dimension along growth axis has large scale. The other six equivalent crystal planes of {111} in the cubic structure also participate in diffraction, but are not influenced by growth orientation. These two features indicate the nanowire growth orientation along one plane of {111}.

The panoramic morphologies of as-obtained GaP (Figure 2A) and InP (Figure 2B) were examined by field emission scanning electron microscopy (FE-SEM), in which the solid samples were mounted on a copper mesh without any dispersion treatment; this indicates that the products consist of nanowires with diameters of 10 nm in average and lengths up to 6 μm. It is worth noting that the yield of InP nanowires (22 %) is much lower than that of the GaP nanowires (56 %), most probably a result of the difficulty in producing $In(OH)_4^-$. More details about the structures of the nanowires were investigated by the electron diffraction (ED) patterns and high-resolution transmission electron microscopy (HRTEM). The HRTEM images and ED patterns of GaP (Figure 2C) and InP (Figure 2D) nanowires show that the as-obtained GaP and InP nanowires are structurally uniform and monocrystalline, growing along [1$\bar{1}$1] and [111] direction, respectively.

The room-temperature (RT) photoluminescence spectra of the as-synthesized GaP and InP nanowires have also been measured. The experiments show the emission of InP

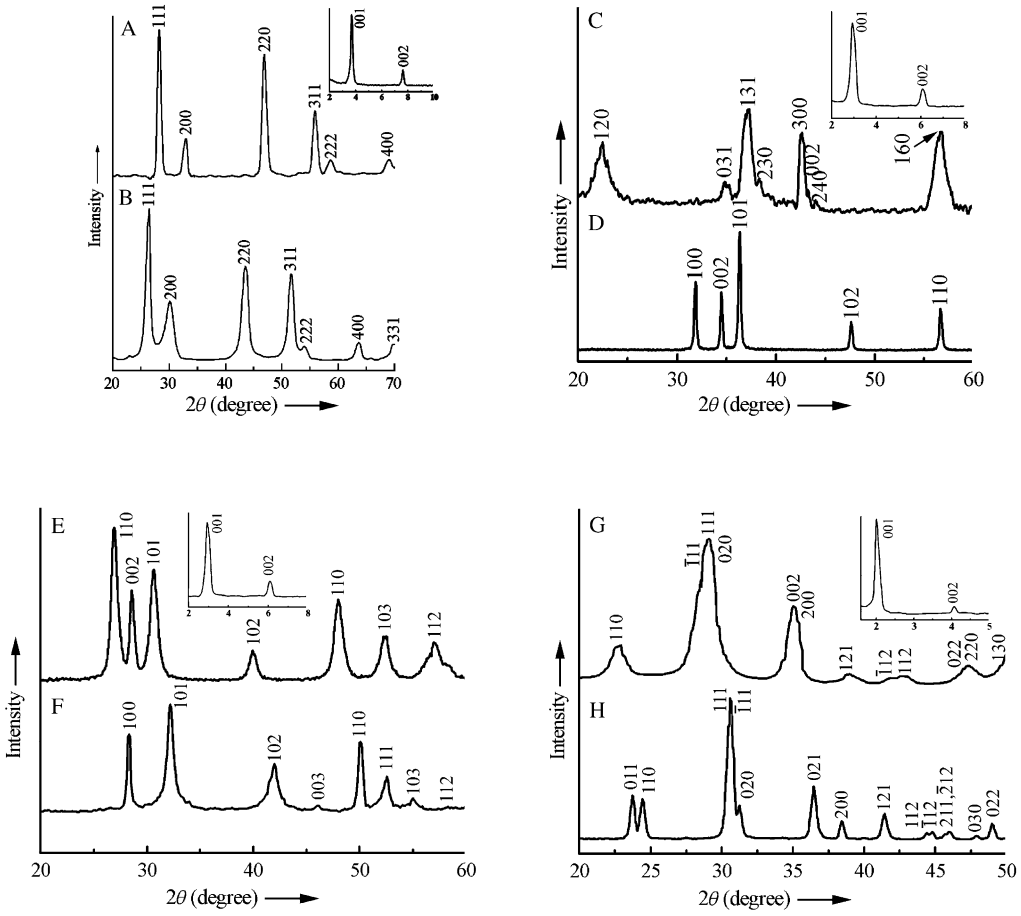

Figure 1. XRD patterns of the as-obtained A) GaP (the inset shows a low-angle XRD pattern of the $[CTA]^+[Ga(OH)_4]^-$ lamellar inorganic–surfactant mesostructures), B) InP, C) γ-MnO_2 (the inset shows a low-angle XRD pattern of the $[CTA]^+[MnO_4^-]$ lamellar inorganic–surfactant mesostructures), D) ZnO, E) ZnS (the inset shows a low-angle XRD pattern of the $[CTA]_2^{2+}[Zn(OH)_4]^{2-}$ lamellar inorganic–surfactant mesostructures), F) SnS_2, G) $CdWO_4$ (the inset shows a low-angle XRD pattern of the $[CTA]_2^{2+}[WO_4]^{2-}$ lamellar inorganic–surfactant mesostructures), and H) $ZnWO_4$ nanowires.

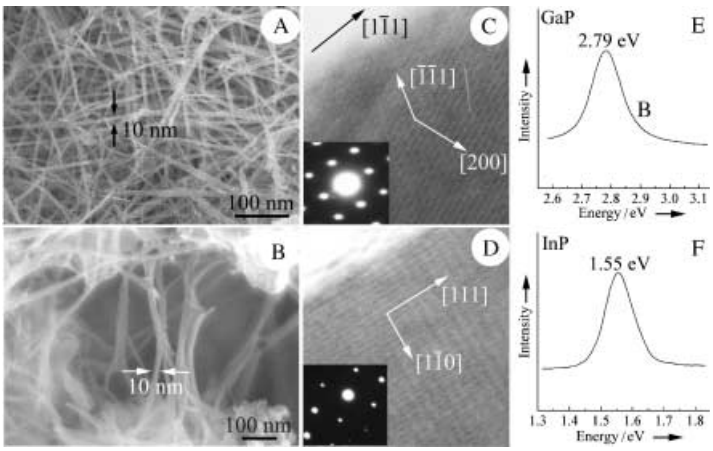

Figure 2. FE-SEM images of the as-grown A) GaP and B) InP nanowires. HRTEM images of the as-grown C) GaP and D) InP nanowires (insets are their ED patterns). Room-temperature photoluminescence spectra of E) GaP and F) InP nanowires.

nanowires (Figure 2E) at 1.55 eV, with a blue-shift of 0.15 eV from the bandgap of bulk InP, resulting from the diameter of 10 nm, which is within the exciton Bohr diameter of InP (19 nm). This is also consistent with the reported data of 10 nm InP nanowires by Lieber et al.[12c] The emission of as-obtained GaP nanowires (Figure 2F) is at 2.79 eV and close to the bandgap of bulk GaP, since their diameters are out of exciton Bohr diameter of GaP (5.5 nm).[17]

The size control of as-obtained nanowires in a certain range can be realized by adjusting some experimental parameters (e.g., amount of $M(OH)_4$, reaction temperature, and time). For example, wirelike assemblies of InP nanoparticles with diameter of approximately 8 nm (Figure 3A)

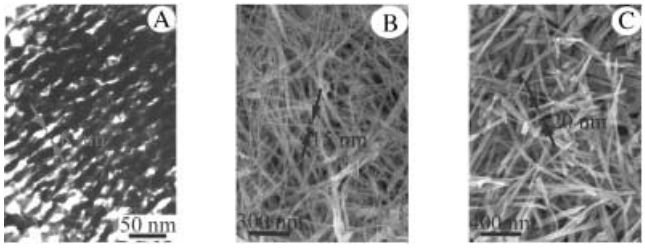

Figure 3. A) TEM image of the as-prepared wire-like assemblies of InP nanoparticles with diameter of approximately 8 nm by decreasing the adding amount of $In(OH)_4^-$. B) and C): FE-SEM images of the as-prepared InP nanowires with diameters of approximately 15 nm and 20 nm at 160 °C for 48 h and 200 °C for 24 h, respectively.

were obtained by decreasing the amount of $In(OH)_4^-$, while other experimental parameters were kept constant; InP nanowires with diameters of approximately 15 nm (Figure 3B) or 20 nm (Figure 3C) were prepared by means of the above designed route at 160 °C for 48 h or 200 °C for 24 h, respectively. Since the diameters of as-obtained InP nanowires are within their exciton Bohr diameter (19 nm),[12c] their size-dependent effects will be evident. From the room-temperature photoluminescence spectra (Figure 4 A), one can see that a systematic shift to higher energy exists as the nanowire diameters are reduced below

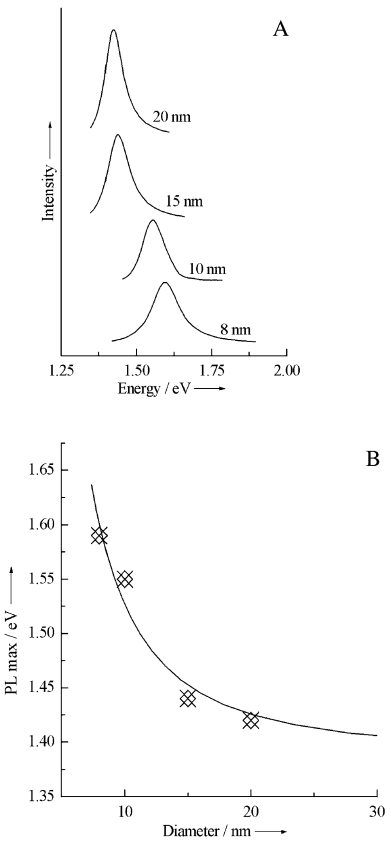

Figure 4. A) Room-temperature photoluminescence spectra of InP nanowires with diameters of 20, 15, 10, and 8 nm. B) Emission energy maxima versus nanowire diameter. The experimental data are fit with EMM (solid line).

20 nm, in agreement with the concept of quantum confinement. The emission energy of InP nanowires with diameters of 20, 15, 10 and 8 nm shifts from 1.42 to 1.59 eV, displaying a size-dependent relationship that is in accordance with the results of Lieber et al.[12c] The size-dependent relationship (Figure 4B) can be fit well with an effective mass model (EMM). The diameters of GaP nanowires are also controllable, but out of exciton Bohr diameter of GaP (5.5 nm), no size-dependent properties can be observed.

Metal oxide: The selected anionic inorganic species to construct lamellar inorganic–surfactant intercalated mesostructures were MnO_4^- and $Zn(OH)_4^{2-}$. The following reactions are designed to grow γ-MnO_2 and ZnO nanowires [Eqs. (4) and (5)].

$$2\,[CTA]^+[MnO_4]^- + 3\,H_2O_2 \rightarrow 2\gamma\text{-}MnO_2 + 2\,H_2O + 3\,O_2 + 2\,OH^- + 2\,CTA^+ \quad (4)$$

$$[CTA]_2^{2+}[Zn(OH)_4]^{2-} \rightarrow ZnO + H_2O + 2\,OH^- + 2\,CTA^+ \quad (5)$$

The inset in Figure 1C shows the low-angle XRD pattern of the $[CTA]^+[MnO_4]^-$ lamellar mesostructures, which were obtained by maintaining the solution of CTAB, $KMnO_4$,

water, *n*-hexanol, and *n*-heptane in an autoclave at 160 °C for 24 h without adding other reactants. The peaks in the low-angle XRD pattern can be indexed as the (001) and (002) reflections of a lamellar mesophase.

The phase and purity of as-obtained product by the present route was determined by the XRD pattern (Figure 1C and D). All the reflection peaks can be indexed to pure orthorhombic γ-MnO_2 (JCPDS card 14–644, $a=6.36$, $b=10.15$, $c=4.09$ Å) and wurtzite ZnO (JCPDS card 36–1451, $a=3.249$, $c=5.206$ Å), respectively. No characteristic peaks were observed for other impurities, such as α-, β-MnO_2, $Mn(OH)_2$, and $Zn(OH)_2$.

The panoramic morphologies of the as-grown γ-MnO_2 and ZnO nanowires were examined by FE-SEM. From Figure 5A, one can see that the diameters of γ-MnO_2 nanowires are 20 nm on average and that their lengths range from 1 μm to 2 μm. Figure 5B shows a typical FE-SEM image of as-grown ZnO nanowires, with diameters of 15 nm and lengths up to 2 μm.

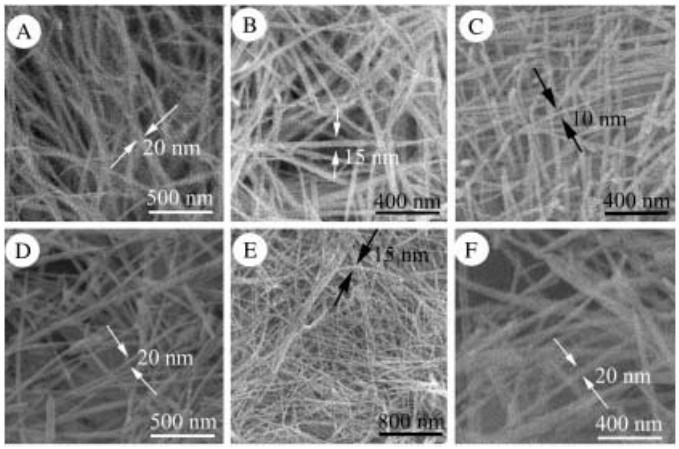

Figure 5. FE-SEM images of the as-grown A) γ-MnO_2, B) ZnO, C) ZnS, D) SnS_2, E) $CdWO_4$, and F) $ZnWO_4$ nanowires.

Metal sulfide: As for the growth of metal sulfide nanowires, we selected $Zn(OH)_4^{2-}$ and $Sn(OH)_6^{2-}$ as the anionic inorganic species to construct lamellar inorganic–surfactant intercalated mesostructures. The reaction can be formulated as follows, taking ZnS as the example [Eq. (6)].

$$[CTA]_2^{2+}[Zn(OH)_4]^{2-} + CH_3CSNH_2 \rightarrow ZnS + CH_3COONH_4 + 2\,OH^- + 2\,CTA^+ \quad (6)$$

The inset in Figure 1E shows the low-angle XRD pattern of the $[CTA]_2^{2+}[Zn(OH)_4]^{2-}$ lamellar mesostructures, which were obtained by maintaining the solution of CTAB, $Zn(OH)_4^{2-}$, water, *n*-hexanol, and *n*-heptane in an autoclave at 160 °C for 48 h without adding other reactants. The peaks in the low-angle XRD pattern can be indexed as the (001) and (002) reflections of a lamellar mesophase.

The phase and purity of as-obtained product by the present route was determined from the XRD pattern (Figure 1E and F). All the reflection peaks can be indexed to pure wurtzite ZnS (JCPDS card 36–1450, $a=3.820$, $c=6.257$ Å) and hexagonal SnS_2 (JCPDS card 23–677, $a=3.648$, $c=5.899$ Å), respectively. No characteristic peaks were observed for other impurities, such as ZnO and SnO_2.

The panoramic morphologies of as-grown ZnS and SnS_2 samples were examined by the FE-SEM. From Figure 5C, we can see that the ZnS samples contain some nanowires with diameters of 10 nm and lengths of approximately 2 μm. Figure 5D shows a typical FE-SEM image of the SnS_2 samples; they show the formation of SnS_2 nanowires with average diameters of 20 nm and lengths ranging from 2 μm to 3 μm.

Metal tungstate: In the above cases, the lamellar compounds provided the metal source for the growth of target nanowires. Further studies reveal that lamellar inorganic–surfactant intercalated mesostructures can also provide anions for the synthesis of oxysalt nanowires. As examples, $CdWO_4$ and $ZnWO_4$ nanowires were grown from lamellar $[CTA]_2^{2+}[WO_4]^{2-}$.

The inset in Figure 1G shows the low-angle XRD pattern of the $[CTA]_2^{2+}[WO_4]^{2-}$ lamellar mesostructures, which were obtained by maintaining the solution of CTAB, WO_4^{2-}, water, *n*-hexanol, and *n*-heptane in autoclave at 160 °C for 48 h without adding other reactants. The peaks in the low-angle XRD pattern can be indexed as the (001) and (002) reflections of a lamellar mesophase.

The phase and purity of as-obtained product from the present route was determined by the XRD (Figure 1G and H) pattern. All the reflection peaks can be indexed to pure monoclinic $CdWO_4$ (JCPDS card 14–676, $a=5.029$, $b=5.859$, $c=5.074$ Å) and monoclinic $ZnWO_4$ (JCPDS card 15–774, $a=3.648$, $c=5.899$ Å), respectively. No characteristic peaks were observed for the other impurities.

The panoramic morphologies of the as-grown $CdWO_4$ and $ZnWO_4$ samples were examined by the FE-SEM. Figure 5E shows a typical FE-SEM image of the $CdWO_4$ samples, showing their rod-like morphologies with an average diameter of 15 nm and lengths of approximately 1.5 μm. From Figure 5F, we can see that the $ZnWO_4$ samples form nanowires with diameters of about 20 nm and lengths up to 2 μm.

The differences in diameter and length of these as-synthesized nanowires should result from the different nature of their corresponding lamellar inorganic–surfactant mesostructures.

Conclusion

In summary, a general synthetic route has been developed for the growth of metal phosphide, oxide, sulfide, and tungstate nanowires in aqueous solution. To the best of our knowledge, this is the first time the synthesis of GaP and InP nanowires in aqueous solution has been achieved. The diameters of as-obtained nanowires are controllable. In particular, the size-dependent properties of InP nanowires are observed. The simple process, general strategy, excellent reproducibility, clean reactions, high yield, and fine quality of products in this work make the present route attractive and

significant. This strategy is expected to extend to the growth of nanowires of other materials by means of solution or vapor transport routes, since the nanowire growth of any inorganic materials can be realized by selecting an appropriate reaction and its corresponding lamellar inorganic–surfactant compounds.

Experimental Section

GaP and InP nanowires: In a typical synthesis, Ga_2O_3 (0.28 g, 1.5 mmol) or In_2O_3 (0.42 g, 1.5 mmol) and NaOH (0.48 g, 12 mmol) were dissolved in distilled water (25 mL). Subsequently, CTAB (1.09 g, 3 mmol), *n*-hexanol (3 mL), and *n*-heptane (10 mL) were added into the solution, which was stirred for 20 min and loaded into a 50 mL Teflon-lined autoclave. Finally, white phosphorus (1.00 g) and I_2 (0.75 g; I_2 was used to transport the produced $H_2PO_2^-$ and accelerate the reactions; this has been described in our previous work[21]) were added into the autoclave, which was then filled with the distilled water up to 90% of the total volume. The autoclave was sealed, warmed up at a speed of 0.5 °C min^{-1} and maintained at 160 °C for 24 h. It was then allowed to cool naturally to room temperature. The precipitate was filtered off, washed with benzene, absolute ethanol, dilute HCl, and distilled water several times, and then dried in vacuum at 60 °C for 4 h.

γ-MnO_2 nanowires: $KMnO_4$ (0.47 g, 3 mmol), CTAB (1.09 g, 3 mmol), *n*-hexanol (3 mL), and *n*-heptane (10 mL) were dissolved in distilled water (25 mL); this solution was stirred for 20 min. Subsequently, 3% H_2O_2 solution was slowly introduced, while magnetic stirring was continued at 50 °C. After completion of the reaction, the solution was loaded into a 50 mL Teflon-lined autoclave, which was then filled with the distilled water up to 90% of the total volume. The autoclave was sealed, warmed up at a speed of 0.5 °C min^{-1} and maintained at 160 °C for 24 h. It was then allowed to cool naturally to room temperature. The precipitate was filtered off, washed with absolute ethanol and distilled water several times, and then dried in vacuum at 60 °C for 4 h.

ZnO nanowires: $Zn(CH_3COO)_2$ (0.33 g, 1.5 mmol) was dissolved in distilled water (25 mL), and then solid NaOH slowly was added and the solution stirred till the pH was about 13. Then the solution was loaded into a 50 mL Teflon-lined autoclave, which was filled with CTAB (1.09 g, 3 mmol), *n*-hexanol (3 mL), *n*-heptane (10 mL), and distilled water up to 90% of the total volume. The autoclave was sealed, warmed up at a speed of 0.5 °C min^{-1} and maintained at 160 °C for 24 h. It was then allowed to cool naturally to room temperature. The precipitate was filtered off, washed with absolute ethanol and distilled water several times, and then dried in vacuum at 60 °C for 4 h.

ZnS and SnS_2 nanowires: $Zn(CH_3COO)_2$ (0.33 g, 1.5 mmol) or $SnCl_4 5H_2O$ (0.53 g, 1.5 mmol) was dissolved in distilled water (25 mL), and then solid NaOH slowly was added and the solution was stirred till the pH was about 13. Subsequently, CTAB (1.09 g, 3 mmol), *n*-hexanol (3 mL), and *n*-heptane (10 mL) were introduced into the solution, which was stirred for 30 min and then loaded into a 50 mL Teflon-lined autoclave. Finally, CH_3CSNH_2 (0.225 g, 3 mmol or 0.375 g, 5 mmol) was added into the autoclave, which was then filled with distilled water up to 90% of the total volume. The autoclave was sealed, warmed up at a speed of 0.5 °C min^{-1} and maintained at 160 °C for 48 or 24 h . It was then allowed to cool naturally to room temperature. The precipitate was filtered off, washed with absolute ethanol and distilled water several times, and then dried in vacuum at 60 °C for 4 h.

$CdWO_4$ and $ZnWO_4$ nanowires: Na_2WO_4 (0.99 g, 1.5 mmol), CTAB (1.09 g, 3 mmol), *n*-hexanol (3 mL), and *n*-heptane (10 mL) were dissolved in distilled water (25 mL); this solution was stirred for 30 min and then loaded into a 50 mL Teflon-lined autoclave. Subsequently, $CdCl_2{\cdot}2.5H_2O$ (0.35 g, 1.5 mmol) or $ZnCl_2$ (0.21 g, 1.5 mmol) was added into the autoclave, which was then filled with the distilled water up to 90% of the total volume. The autoclave was sealed, warmed up at a speed of 0.5 °C min^{-1} and maintained at 160 °C for 48 or 24 h. It was then allowed to cool naturally to room temperature. The precipitate was filtered off, washed with absolute ethanol and distilled water several times, and then dried in vacuum at 60 °C for 4 h.

Characterization: X-ray diffraction (XRD) patterns were performed with a Japan Rigaku D/max γA X-ray diffractometer equipped with graphite monochromatized high-intensity $Cu_{K\alpha}$ radiation ($\lambda = 1.54178$ Å), in which the sample of small amount was not ground, but fully dispersed with ethanol. Field emission scanning electron microscopy (FE-SEM) images were recorded on a JEOL JSM-6700F SEM. High-resolution transmission electron microscopy (HRTEM) images and electronic diffraction (ED) patterns were carried out on a JEOL-2010 TEM at an acceleration voltage of 200 KV. UV/Vis spectra were recorded on a JGNA Specord 200 PC UV/Vis spectrophotometer. The room-temperature photoluminescence spectra were collected on a Jobin Yvon-Labram spectrometer with an He–Cd laser.

Acknowledgement

This work was supported by the Chinese National Natural Science Foundation. The authors thank Prof. Shuyuan Zhang and Ke Jiang for technical assistance in HRTEM and FE-SEM experiments.

[1] a) A. P. Alivisatos, *Science* **1996**, *271*, 933; b) A. M. Morales, C. M. Lieber, *Science* **1998**, *279*, 208.
[2] a) Y. Zhou, S. H. Yu, X. P. Cui, C. Y. Wang, Z. Y. Chen, *Chem. Mater.* **1999**, *11*, 545; b) J. J. Zhu, S. W. Liu, O. Palchik, Y. Koltypin, A. Gedanken, *Langmuir* **2000**, *16*, 6396; c) D. Xu, Y. Xu, D. Chen, G. Guo, L. Gui, Y. Tang, *Adv. Mater.* **2000**, *12*, 520.
[3] a) C. R. Martin, *Science* **1994**, *226*, 1961; b) M. H. Huang, A. Choudrey, P. D. Yang, *Chem. Commun.* **2000**, 1063.
[4] a) S. Bhattacharrya, S. K. Saha, D. Chakravorty, *Appl. Phys. Lett.* **2000**, *76*, 3896; b) S. W. Liu, J. Yue, A. Gedanken, *Adv. Mater.* **2001**, *13*, 656; c) S. Bhattacharrya, S. K. Saha, D. Chakravorty, *Appl. Phys. Lett.* **2000**, *77*, 3770; d) N. R. Jana, L. Gearheart, C. L. Murphy, *Chem. Commun.* **2001**, 617.
[5] a) S. Iijima, *Nature* **1991**, *354*, 56; b) T. Seeger, P. Kohler-Redlich, M. Ruhle, *Adv. Mater.* **2000**, *12*, 279.
[6] a) A. M. Morales, C. M. Lieber, *Science* **1998**, *279*, 208; b) M. S. Gudiken, C. M. Lieber, *J. Am. Chem. Soc.* **2000**, *122*, 8801.
[7] a) Y. Sun, B. Gates, B. Mayers, Y. Xia, *Nano Lett.* **2002**, *2*, 165; b) B. Gates, Y. Yin, Y. Xia, *J. Am. Chem. Soc.* **2000**, *122*, 12582.
[8] Y. Wu, P. Yang, *Chem. Mater.* **2000**, *12*, 605.
[9] a) K. Soulantica, A. Maisonnat, F. Senocq, M. C. Fromen, M. J. Casanove, B. Chaudret, *Angew. Chem.* **2001**, *113*, 3071; Angew. Chem. Int. Ed. **2001**, *40*, 2984; b) Y. J. Xiong, Y. Xie, Z. Q. Li, C. Z. Wu, *Chem. Eur. J.* **2003**, *9*, 1645; c) Y. J. Xiong, Y. Xie, Z. Q. Li, R. Zhang, J. Yang, C. Z. Wu, *New J. Chem.* **2003**, *27*, 588; d) Y. J. Xiong, Z. Q. Li, R. Zhang, Y. Xie, J. Yang, C. Z. Wu, *J. Phys. Chem. B* **2003**, *107*, 3697.
[10] Y. N. Xia, P. D. Yang, Y. G. Sun, Y. Y. Wu, B. Mayers, B. Gates, Y. D. Yin, F. Kim, Y. Q. Yan, *Adv. Mater.* **2003**, *15*, 353.
[11] a) H. Morkoc, S. N. Mohammad, *Science* **1995**, *267*, 51; b) H. Morkoc, S. Strite, G. B. Gao, M. E. Lin, B. Sverdlov, M. Burns, *J. Appl. Phys.* **1994**, *76*, 1363; c) T. Matsuoka, T. Ohki, T. Ohno, Y. Kawaguchi, *J. Cryst. Growth* **1994**, *138*, 727.
[12] a) M. S. Gudiksen, J. Wang, C. M. Lieber, *J. Phys. Chem. B* **2001**, *105*, 4062; b) W. S. Shi, Y. F. Zheng, N. Wang, C. S. Lee, S. T. Lee, *J. Vac. Sci. Technol. B* **2001**, *19*, 1115; c) M. S. Gudiksen, J. Wang, C. M. Lieber, *J. Phys. Chem. B* **2002**, *106*, 4036.
[13] S. C. Lyu, Y. Zhang, H. Ruh, H. J. Lee, C. J. Lee, *Chem. Phys. Lett.* **2003**, *367*, 717.
[14] H. W. Seo, S. Y. Bae, J. Park, H. Yang, S. Kim, *Chem. Commun.* **2002**, 2564.
[15] C. Tang, S. Fan, M. Lamy de la Chapelle, H. Dang, P. Li, *Adv. Mater.* **2000**, *12*, 1346.
[16] T. J. Trentler, K. M. Hickman, S. C. Goel, A. M. Viano, P. C. Gibbons, W. E. Buhro, *Science* **1995**, *270*, 1791.
[17] Y. H. Kim, Y. W. Jun, B. H. Jun, S. M. Lee, J. Cheon, *J. Am. Chem. Soc.* **2002**, *124*, 13656.
[18] S. Kan, T. Mokari, E. Rothenberg, U. Banin, *Nat. Mater.* **2003**, *2*, 155.

[19] a) M. P. Zach, K. H. Ng, R. M. Penner, *Science* **2000**, *290*, 2120; b) S. Morin, A. Lachenwitzer, O. M. Magnussen, R. J. Behm, *Phys. Rev. Lett.* **1999**, *83*, 5066.
[20] a) Y. Li, X. Li, Z. X. Deng, B. Zhou, S. Fan, J. Wang, X. Sun, *Angew. Chem.* **2002**, *114*, 343; *Angew. Chem. Int. Ed.* **2002**, *41*, 333; b) Y. Li, X. Li, Z. X. Deng, B. Zhou, S. Fan, J. Wang, X. Sun, *Angew. Chem.* **2002**, *114*, 343.
[21] S. Gao, J. Lu, Y. Zhao, N. Chen, Y. Xie, *Chem. Commun.* **2002**, 3064.

Received: September 24, 2003 [F5569]